Letter

Determining the Energy Gap between the S_1 and T_1 States of Thermally Activated Delayed Fluorescence Molecular Systems Using Transient Fluorescence Spectroscopy

Min Zheng,[∥] Yuanming Li,[∥] Yaxiong Wei, Lin Chen,* Xiaoguo Zhou,* and Shilin Liu

Read Online

ACCESS | Metrics & More | Article Recommendations | SI Supporting Information

ABSTRACT: The energy gap (ΔE_{S-T}) between the lowest single and triple excited states is a crucial parameter for thermally activated delayed fluorescence (TADF) molecular systems with high quantum yield. However, a reliable experimental approach to precisely determine this value is challenging. Here, we introduce a new, simple, and efficient strategy to accurately obtain the ΔE_{S-T} in TADF systems from time-resolved fluorescence spectroscopy using a recently reported TADF molecule, DMACPDO, as a representative. By introducing an explicit model to describe the corresponding singlet−triplet coupling system, elusive intersystem crossing and reverse intersystem crossing rates can be extracted by fitting the kinetics of the observed fluorescence. The ΔE_{S-T} value can then be determined. Moreover, our modeling accurately explained the opposite trend in fluorescence intensity of DMACPDO with solvent polarity under air-saturated and deoxygenated conditions. Additionally, the validity of this approach has been demonstrated in another well-known TADF molecule, 4CzIPN. We demonstrate how this approach of determining ΔE_{S-T} sheds light on a deeper understanding of energy-loss mechanisms involved in related photoconversion processes.
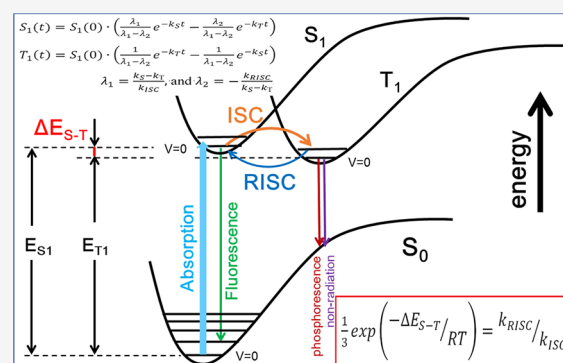
Thermally activated delayed fluorescence (TADF) has attracted considerable interest because of its ability to enhance the efficiency of organic light-emitting diodes (OLEDs) by harvesting triplet excitons. For a TADF molecular system, the energy gap (ΔE_{S-T}) between the lowest single (S_1) and triple (T_1) excited states is the most crucial parameter for achieving a high quantum yield (or the efficiency) of delayed fluorescence emission.[1−8] An overall TADF process has been extensively addressed in the context of the Jablonski diagram, as shown in Figure 1. Usually, the smaller the ΔE_{S-T}, the greater the TADF efficiency, which has proven vital for the improvement of OLED efficiency.[4,9−13] With a smaller ΔE_{S-T} (usually less than 100 meV),[4] both singlet-to-triplet intersystem crossing (ISC) and reverse ISC (RISC) have fast reaction rates, thus establishing an equilibrium between the S_1 and T_1 state populations. Following photoexcitation, fluorescence emission occurs immediately from the populated S_1 state, also called prompt fluorescence (PF). Also, activated excitons in the T_1 state are reversely converted to S_1 via a thermally activated process due to the equilibrium, resulting in extra fluorescence emission. Since this endothermic RISC is relatively slow compared with the exothermic ISC, the fluorescence emits later than the PF emission and is therefore called delayed fluorescence (DF).

In theory, ΔE_{S-T} is defined as the energy difference between the S_1 and T_1 states at each optimized geometry (i.e., $\Delta E_{S-T} =$

$E_{S1} - E_{T1}$, where E_{S1} and E_{T1} are the adiabatic excitation energies of the $S_1(\nu = 0)$ and $T_1(\nu = 0)$ levels. Although this definition is clear, the accurate experimental determination of ΔE_{S-T} remains challenging; hence, a few crude approximations have been widely used in early studies.[14] For example, the E_{S1} value is usually estimated using steady-state absorption and fluorescence spectroscopy.[14] Based on the Franck−Condon principle, the ideal 0−0 transition energy of S_1 (so-called E_{S1}) corresponds to the lowest energy onset in the absorption spectra or the highest energy threshold of the fluorescence spectra when these absorptions and emissions occur solely for discrete photon energies related to transitions between the vibrational levels of the ground and excited states. However, the absorption and emission spectra of photosensitizers seldom consist of well-resolved vibrational peaks due to low-frequency vibrations and electron−phonon coupling. Thus, transitions from thermally populated vibrational modes always lead to the onset of absorption at photon energies below E_{S1} and emission at energies above E_{S1}. Besides, the E_{T1} value (0−0 transition
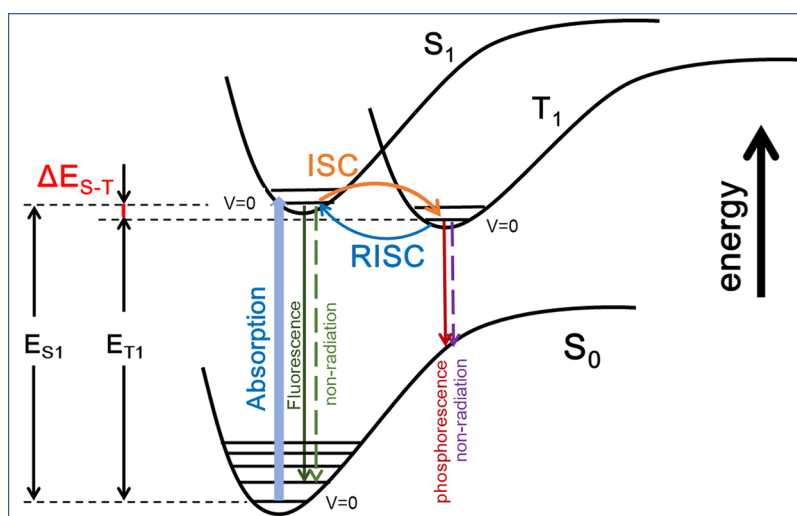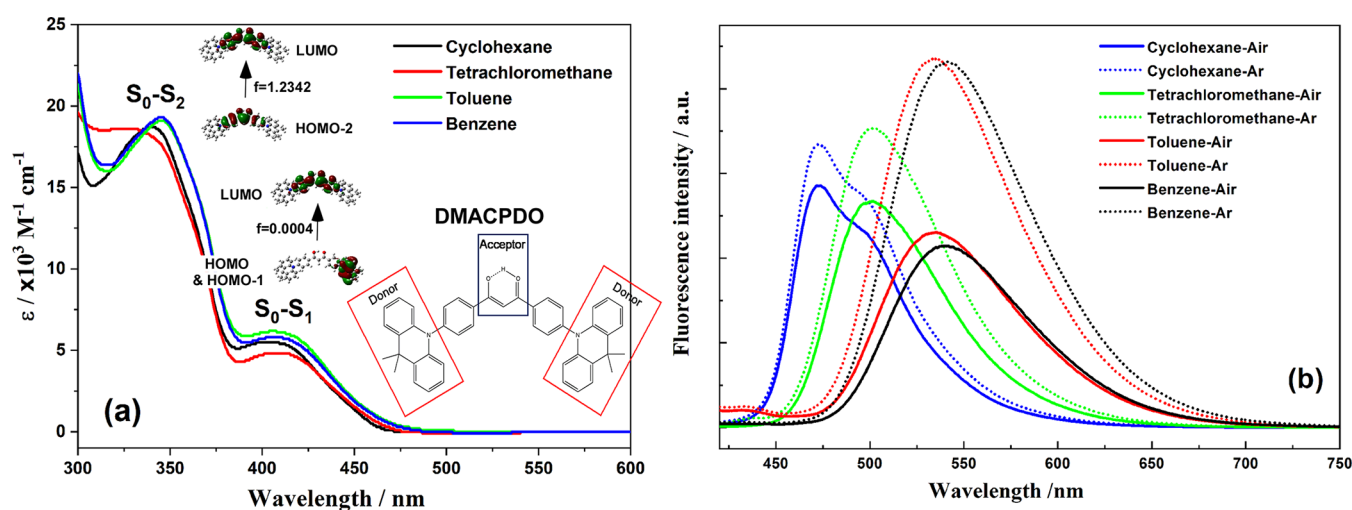
Figure 1. Jablonski diagram of a representative thermally activated delayed fluorescence process. ISC indicates intersystem crossing, and RISC is reverse intersystem crossing. S_1 and T_1 represent the lowest singlet and triplet excited states, respectively.

Figure 2. (a) Steady-state UV−vis absorption and (b) fluorescence emission (λ_{ex} = 405 nm) spectra of DMACPDO in cyclohexane, tetrachloromethane, toluene, and benzene solvents (1×10^{-5} M) at room temperature.

energy of T_1) has been assessed as the highest-energy threshold onset of low-temperature (77 K) phosphorescence spectra,[6,15−20] and the peak maximums of both fluorescence and phosphorescence spectra have been used to evaluate E_{S1} and E_{T1} in a few experiments.[21,22] Apparently, these methods are far from accurate measurements. Recently, Vandewal et al. proposed a simple but efficient strategy to precisely determine E_{S1} as the crossing point of appropriately normalized absorption and emission spectra.[23] In contrast, no reliable experimental approach has been reported to precisely determine the E_{T1} value. Moreover, using the temperature-dependent photoluminescence measurements, the $\Delta E_{S−T}$ value was estimated by fitting the plot of the photoluminescence lifetime vs temperature.[24−27] However, there was a very stringent condition in this method, that the prompt fluorescence is entirely quenched and cannot be observed directly due to the much faster ISC rate than the fluorescence emission rate, and thus, the luminescence in experiment is only contributed by the delayed fluorescence component. Apparently, it is not suitable for every TADF molecular system.

Relative to experiments, theoretical calculations have made great progress in predicting excitation energies in past decades.[28−31] Density functional theory (DFT) and time-dependent DFT (TD-DFT)[32−34] have been widely used to calculate $\Delta E_{S−T}$ because of the favorable trade-off between accuracy and computational cost.[35] The average uncertainties are generally in a range of 0.1−0.3 eV[36−40] with the classical DFT and TD-DFT methods. Recently, the development of optimally tuned range-separated density functionals makes a certain improvement in predicting $\Delta E_{S−T}$ with mean absolute deviations of 0.09 eV.[41] However, in these range-separated exchange density functionals, the range-separation parameters are strongly system-dependent, constraining their wide application. Additionally, Penfold proposed a simple analysis based on the overlap between the highest occupied molecular orbital (HOMO) and the lowest unoccupied molecular orbital (LUMO) to estimate $\Delta E_{S−T}$.[42] The mean errors relative to the reported experimental values were reduced to 0.05 eV. Nevertheless, such uncertainties still cannot meet the rigorous demand for $\Delta E_{S−T}$ to predict the ISC and RISC rates of TADF molecules.[4,43]

For most TADF molecules, the S_1 or T_1 state is often accompanied by moderate changes in molecular geometry relative to the ground state, with certain characteristics of charge-transfer (CT) states. Their spectra contain no fine vibrational structures, regardless of their fluorescence and phosphorescence emissions. Moreover, most solvents are glassy during low-temperature (77 K) measurements, in which the solvation energy is different from that at room temperature due to the exceptionally postponed relaxation time of solvent molecules.[44,45] In other words, the E_{T1} value estimated from spectra under the glassy condition may be inevitably shifted from its real state at room temperature. Therefore, the fundamental understanding of the TADF process requires an unambiguous experimental approach to precisely determine the ΔE_{S-T} and E_{T1} values.

Recently, an excited-state intramolecular proton transfer (ESIPT) emitter, DMACPDO, has been synthesized with high photoluminescence quantum yield (86%) and a relatively long fluorescence lifetime (1.94 μs) in the film state.[16] In its symmetric D-π-A-π-D molecular architectures (see the inserted structure in Figure 2a), 9,9-dimethyl-9,10-dihydroacridine (DMAC) and β-diketone moieties play the roles of electron donor (D) and electron acceptor (A), respectively. The D and A subunits are connected through phenylene π-bridges, and each D-π-A unit has a twisting configuration. The sole enol-type forms stabilized by intramolecular hydrogen bonds together with the twisting configuration of the D and A moieties promote its TADF characteristics.[16] However, the core parameter, ΔE_{S-T}, has not been determined by either experiment or calculation. Thus, this new strategy for designing efficient ESIPT emitters has limited significance.

In this work, we proposed an experimental approach using ultrafast kinetic measurements to precisely determine ΔE_{S-T} using DMACPDO as an example. We observed and explained the unusual dependence of prompt and delayed fluorescence intensities on solvent polarity based on time-resolved fluorescence spectra and kinetics. For comparison, theoretical calculations using standard DFT and TD-DFT were also performed for the S_0, S_1, and T_1 electronical states of DMACPDO.

As the HOMO and LUMO of the DMACPDO molecule are dominantly localized on the D and A units, respectively, an intramolecular CT process naturally occurs upon photoexcitation. Accordingly, the CT state energy might be sensitive to the fraction of Hartree–Fock exchange in hybrid functionals; thus, we performed a series of computations for the UV−vis absorption and fluorescence emission spectra of DMACPDO at several different DFT levels (e.g., B3LYP,[46,47] PBE0,[48,49] BMK,[50] M062X,[51,52] CAM-B3LYP,[53] and ωB97XD[54]). The polarizable continuum model (PCM) model[34,55] was used to describe solvent effects on equilibrium geometries and excitation energies. As the calculated results at these levels were generally consistent, as shown in the Supporting Information, we only present the BMK results here as a representative. Once excited, the dihedral angle between the Ph-bridge and acceptor in DMACPDO is significantly decreased from 17° in S_0 to approximately 0° in S_1, while the dihedral angle between the donor and the Ph-bridge is maintained at ∼90°. Such a large change in the dihedral angle between D−A units reduces the overlap of frontier orbitals, leading to a reduced ΔE_{S-T} value and the good performance of DMACPDO as an ideal TADF molecule. In addition, the optimized geometries of the S_0, S_1, and T_1

states in cyclohexane, tetrachloromethane, toluene, and benzene solvents are very close at all of these theoretical levels. Therefore, no apparent solvent effects were predicted for the calculated excitation energies of E_{S1} and E_{T1}, as shown in Table S1 of the Supporting Information. As a result, the ΔE_{S-T} values in these four solvents were computed to be in the range of 0.17−0.25 eV.

The steady-state UV−vis absorption spectra of DMACPDO in cyclohexane, tetrachloromethane, toluene, and benzene exhibited very similar features, as shown in Figure 2a: a weak band ($S_0 \rightarrow S_1$) contributed by the HOMO (or HOMO$_{-1}$) $\rightarrow$ LUMO transition at ∼405 nm and a $\pi−\pi^*$ transition (HOMO$_{-2} \rightarrow$ LUMO) located at ∼340 nm ($S_0 \rightarrow S_2$). Notably, the HOMO and HOMO$_{-1}$ are degenerated due to the almost symmetric D−A−D structure. With the increase in solvent polarity, the two absorption peaks showed mild red-shifts, indicating that the dipole moments of the S_1 and S_2 states were slightly larger than that of the ground state S_0. Figure 2b shows the overall fluorescence emission spectra of DMACPDO in the four solvents, with photoexcitation at 405 nm ($S_0 \rightarrow S_1$). Unlike the absorption spectra and the prediction of the preceding quantum calculation, the fluorescence emission peak exhibited a significant red-shift with increasing solvent polarity, which was consistent with the CT feature of S_1. To our surprise, the trend in the dependence of fluorescence intensity on solvent polarity was opposite in the presence and absence of solvated oxygen, as indicated by the solid and dashed curves in Figure 2b. The fluorescence yield (Φ_F) under air-saturated conditions was visibly reduced with increasing solvent polarity (e.g., 10.94% in tetrachloromethane and 9.37% in benzene). Contrastingly, a positive correlation with solvent polarity was observed in the fluorescence intensity in deoxygenated solutions. The Φ_F value was significantly enhanced from 10.30% in cyclohexane to 14.57% in tetrachloromethane, 17.32% in toluene, and 18.90% in benzene (Table 1). Additionally, the overall

**Table 1. Absorption and Fluorescence Emission of DMACPDO in Four Solvents at Room Temperature**

solvent	dielectric constant	λ_{abs} (nm)	ε (M^{-1}·cm^{-1})	λ_{em} (nm)	$\Phi_F{}^a$ (%)
cyclohexane	2.052	405	5500	470	10.30
tetrachloromethane	2.238	407	4800	495	14.57
toluene	2.240	406	6200	550	17.32
benzene	2.283	412	5800	550	18.90

^{a}Measured in deoxygenated solutions.

fluorescence intensities in the deoxygenated solutions were stronger than those in the air-saturated solutions, as shown in Figure 2b. This inconsistent dependence in the presence and absence of solvated oxygen provided indubitable evidence for the existence of a DF component in the observed fluorescence emission according to the quenching of solvated oxygen molecules.

Usually, the steady-state fluorescence of a TADF molecule includes a simultaneous PF component with a short lifetime (from a picosecond to a few tens of nanoseconds) and a DF component with a long lifetime (microseconds), where the latter mainly originated from a thermally activated RISC from nearby triplet states. For DMACPDO in air-saturated solutions, the T_1 state is efficiently quenched by solvated oxygen; hence, only the PF process contributes to the observed

fluorescence. In comparison, the fluorescence in the deoxygenated solutions involves both PF and DF components. Therefore, the opposite dependences of fluorescence intensity on solvent polarity in the presence and absence of solvated oxygen strongly imply that solvent polarity plays a crucial role in the thermally activated RISC of DMACPDO by changing ΔE_{S-T}. With increasing solvent polarity, the ΔE_{S-T} value should reduce to accelerate ISC and RISC, which leads to a higher populated T_1 state and improves the fraction of the DF component. To quantitatively characterize the fractions of the PF and DF components and precisely determine their lifetimes, the transient fluorescence kinetics of DMACPDO in these solvents was measured. As shown in Figure 3, the
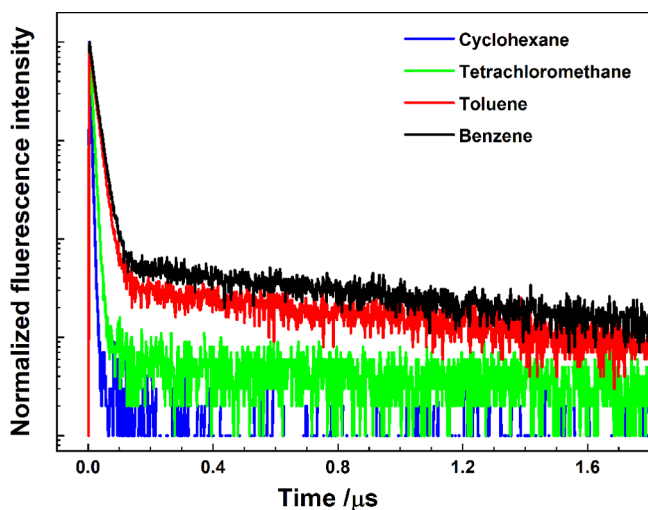
Figure 3. Fluorescence emission kinetics for DMACPDO (1×10^{-5} M) in deoxygenated cyclohexane, tetrachloromethane, toluene, and benzene solvents at room temperature and $\lambda_{ex} = 375$ nm.

fluorescence decay kinetics is typically comprised of two processes: a fast nanosecond PF and a slow microsecond DF. By fitting these biexponential curves and integrating the corresponding fluorescence intensities in different characteristic time domains, the proportions of the PF and DF components (I_{PF}/I_{DF}) were calculated. Table 2 lists the

Table 2. Lifetimes of the Prompt Fluorescence (PF) and Delayed Fluorescence (DF) Components of DMACPDO in Four Solvents at Room Temperature, as Well as the Proportion of Their Intensities

solvent	τ_{PF} (ns)	τ_{DF} (ns)	I_{PF}/I_{DF}
cyclohexane	3.51 ± 0.02	a	~0.99/0.01
tetrachloromethane	6.89 ± 0.01	2640 ± 127	0.89/0.11
toluene	15.46 ± 0.01	1039 ± 25	0.82/0.18
benzene	17.51 ± 0.01	1100 ± 16	0.76/0.24

^{a}Too weak to be obtained from fitting.

lifetimes and the relative proportions of the PF and DF components in the four deoxygenated solvents. The PF lifetime was gradually extended from 3.51 ns in cyclohexane to 17.51 ns in benzene, with increasing solvent polarity, while the DF lifetime decreased (i.e., 2640 ns in tetrachloromethane, 1039 ns in toluene, and 1100 ns in benzene). Notably, the fraction of the DF component of the overall fluorescence

intensity is visibly promoted by solvent polarity, while its corresponding lifetime is shortened.

According to the Jablonski diagram shown in Figure 1, the PF emission and the ISC process are in competition. Since the PF emission rate is reduced with increasing solvent polarity, as indicated by τ_{PF} in Table 2, the promotion of the DF fraction in polar solvents suggests that the ISC becomes more favorable with increased rate; thus, the ΔE_{S-T} value in polar solvents should naturally decrease with solvent polarity. Following this deduction, it is predicted that the triplet lifetime can be reduced by increasing solvent polarity owing to accelerated RISC, which is greatly consistent with the present experimental results. To quantitatively examine this prediction and determine the ΔE_{S-T} value, we conducted population-evolution modeling for the decay of an excited DMACPDO molecule after photoexcitation based on the Jablonski diagram. Fluorescence emission, ISC, and RISC processes were included for the decay and formation of the singlet excited state, while internal conversion (IC) was considered insignificant in this system according to the energy gap law[56] and the too-large energy gap between S_1 and S_0 states (i.e., 52−70 kcal/mol, as derived from the absorption peak in Figure 2a). Additionally, other non-radiation decay pathways, such as collision, were also neglected for the S_1 state compared to the fluorescence emission and ISC. A similar assumption was made for the evolution of the T_1 state population formed by the ISC from S_1; that is, IC was removed from the modeling. Meanwhile, phosphorescence emission was assumed to be insignificant for the T_1 state, since no phosphorescence was observed in the room-temperature experiments. Additionally, unlike the case of S_1, the non-radiation pathway, such as collision, may have been indispensable for the T_1 population according to its relatively long lifetime. Consequently, only RISC and non-radiation pathways were included for the T_1 decay. Therefore, the time-dependent singlet and triplet populations, denoted $S_1(t)$ and $T_1(t)$, respectively, can be described by the following equations

$$\frac{dS_1(t)}{dt} = -(k_{ISC} + k_F) \cdot S_1(t) + k_{RISC} \cdot T_1(t)$$
$$= -k_S \cdot S_1(t) + k_{RISC} \cdot T_1(t) \tag{1}$$

$$\frac{dT_1(t)}{dt} = k_{ISC} \cdot S_1(t) - (k_{RISC} + k_{NR}^T) \cdot T_1(t)$$
$$= k_{ISC} \cdot S_1(t) - k_T \cdot T_1(t) \tag{2}$$

where k_{ISC}, k_{RISC}, k_F, and k_{NR}^T denote the elementary rates of the ISC, RISC, fluorescence emission, and non-radiation pathways, respectively, and $k_S = k_{ISC} + k_F$ and $k_T = k_{RISC} + k_{NR}^T$ are the overall decay rates of the S_1 and T_1 states. As for TADF systems[4,57,58] and also well justified in the current experiments (as described in the following discussions), a certain approximation, $k_{ISC} \gg k_{RISC}$ (or k_{NR}^T), was adopted, and hence, $k_S \gg k_T$ was achieved. Jointly solving eqs 1 and 2 gives the following simplified, analytical expressions

$$S_1(t) = S_1(0) \cdot \left(\frac{\lambda_1}{\lambda_1 - \lambda_2} e^{-k_S t} - \frac{\lambda_2}{\lambda_1 - \lambda_2} e^{-k_T t} \right) \tag{3}$$

$$T_1(t) = S_1(0) \cdot \left(\frac{1}{\lambda_1 - \lambda_2} e^{-k_T t} - \frac{1}{\lambda_1 - \lambda_2} e^{-k_S t} \right) \tag{4}$$

Table 3. Dynamic Decay Parameters for DMACPDO in the S_1 State at Room Temperature Derived from the Fitting of Fluorescence Intensity Curves

solvent	k_S ($\times 10^7$ s^{-1})	k_T ($\times 10^5$ s^{-1})	$\dfrac{\lambda_1}{\lambda_1 - \lambda_2}$	$-\dfrac{\lambda_2}{\lambda_1 - \lambda_2}$	$k_{ISC} \cdot k_{RISC}$ ($\times 10^{13}$ s^{-2})
cyclohexane	28.57 ± 0.16				
tetrachloromethane	14.50 ± 0.01	3.79 ± 0.18	19748	7	0.74
toluene	6.47 ± 0.01	9.63 ± 0.23	13186	44	1.36
benzene	5.71 ± 0.01	9.09 ± 0.13	12728	67	1.66

Table 4. Dynamic Decay Parameters of DMACPDO (S_1) in Deoxygenated Solutions at Room Temperature

solvent	k_F ($\times 10^6$ s^{-1})	k_{ISC} ($\times 10^7$ s^{-1})	k_{RISC} ($\times 10^5$ s^{-1})	k_{NR}^T ($\times 10^5$ s^{-1})	ΔE_{S-T} (eV)
cyclohexane	29.10 ± 3.20	25.70 ± 0.36			
tetrachloromethane	18.80 ± 2.58	12.62 ± 0.26	0.59 ± 0.02	3.20 ± 0.18	0.17 ± 0.01
toluene	9.19 ± 1.00	5.55 ± 0.10	2.44 ± 0.07	7.18 ± 0.31	0.11 ± 0.01
benzene	8.20 ± 0.84	4.89 ± 0.08	3.40 ± 0.08	5.69 ± 0.16	0.10 ± 0.01

where $S_1(0)$ is the initial concentration of the S_1 state ($t = 0$), $\lambda_1 = \frac{k_S - k_T}{k_{ISC}}$, and $\lambda_2 = -\frac{k_{RISC}}{k_S - k_T}$. The details of the above formulations are given in the Supporting Information. Therefore, both $S_1(t)$ and $T_1(t)$ populations exhibit a form of biexponential decay after photoexcitation in exact agreement with the kinetics shown in Figure 3. In the current study, the evolution of the $T_1(t)$ population was not detected due to a lack of low-temperature phosphorescence measurement apparatus; however, the observed fluorescence decay dynamics clearly shows the relationship between the $S_1(t)$ population and decay time. Thus, the values of k_S and k_T are directly obtained by fitting the routine kinetics shown in Figure 3 with eq 3. Two pre-exponential coefficients, $\frac{\lambda_1}{\lambda_1 - \lambda_2}$ and $-\frac{\lambda_2}{\lambda_1 - \lambda_2}$, are also determined. Detailed comparisons of the experimental and fitted results for the four solvents are given in Figure S1 of the Supporting Information. Given that it is not possible to directly extract the λ_1 and λ_2 coefficients from this fitting, here we introduce a new approach to obtain k_{ISC} and k_{RISC} values. Specifically, the $k_{ISC} \cdot k_{RISC}$ value can be calculated by dividing these two pre-exponential coefficients. Table 3 lists all of the obtained dynamic parameters for the four solvents.

During the initial fluorescence emission stage, the contribution of the DF component can be ignored due to a limited T_1 population. Thus, the quantum yield of the PF process, Φ_{PF}, is readily calculated by eq 5 according to the Jablonski diagram. Meanwhile, Φ_{PF} could also be estimated from eq 6 as a part of the overall fluorescence quantum yield, Φ_F, from the experiments.

$$\Phi_{PF} = k_F / (k_F + k_{ISC}) = k_F / k_S \tag{5}$$

$$\Phi_{PF} = \Phi_F \cdot [I_{PF} / (I_{PF} + I_{DF})] \tag{6}$$

Using the experimentally measured Φ_F and I_{PF}/I_{DF} data in Table 1 together with the k_S values in Table 3, k_F and k_{ISC} can be calculated. We can then obtain k_{RISC} values for the different solvents based on the $k_{ISC} \cdot k_{RISC}$ values in Table 3. Additionally, the k_{NR}^T values of non-radiation rates for the T_1 state are subsequently determined as the difference between k_T and k_{RISC}. Table 4 summarizes these calculated values. Take toluene, for instance, the k_F, k_{ISC}, k_{RISC}, and k_{NR}^T values are 9.19 $\times 10^6$, 5.55 $\times 10^7$, 2.44 $\times 10^5$, and 7.18 $\times 10^5$ s^{-1}, respectively. In fact, these values agree with our assumptions of $k_{ISC} \gg k_{RISC}$ and $k_{ISC} \gg k_{NR}^T$.

As shown in Table 2, the typical value of τ_{DF} is larger than 1 μs; therefore, thermal dynamic equilibrium between the S_1 and T_1 populations can be rapidly established[59] (usually in a time scale of picoseconds to nanoseconds) at room temperature after the initial photoexcitation, with the triplet state being activated, and keeping both the S_1 and T_1 populations in a type of steady-state. As indicated in Figure S2 of the Supporting Information, this reversible process takes only about 60 ns to establish equilibrium using the obtained k_S and k_T values. Therefore, the ΔE_{S-T} value can be calculated using the following equation based on this equilibrium approximation

$$\frac{1}{3} \exp(-\Delta E_{S-T} / RT) = k_{RISC} / k_{ISC} \tag{7}$$

where T is the ambient temperature. At room temperature (298 K), the calculated ΔE_{S-T} values using the above k_{ISC} and k_{RISC} data are listed in Table 4. The ΔE_{S-T} value of DMACPDO does decrease with increasing solvent polarity (e.g., 0.17 eV for tetrachloromethane, 0.11 eV for toluene, and 0.10 eV for benzene) in perfect agreement with our experimental results. Additionally, the calculated ΔE_{S-T} values using the standard DFT or TD-DFT methods, such as BMK, are 0.17−0.18 eV, which are acceptable considering the uncertainty of the calculated levels of the theory, yet they do not exhibit a similar trend with solvent polarity. This disagreement further indicates that these standard DFT approaches and the PCM model are insufficient to quantify ΔE_{S-T}. Lastly, Hu et al. very recently have demonstrated a novel approach for the facile retrieval of a RISC rate from the global kinetics fitting of transient absorption spectra.[60] They were able to readily calculate the ΔE_{S-T} value of a corresponding rare-earth chelate molecular system based on their k_{ISC} and k_{RISC} data. Nevertheless, it is worth noting that, in their systems, the dominant decay of a singlet excited photosensitizer is ultrafast ISC (i.e., $k_{ISC} = 0.235$ ps^{-1}),[60] while fluorescence emission and other non-radiation paths are negligible. Moreover, intramolecular resonance energy transfer plays the same crucial role as RISC in the evolution of the T_1 population compared to TADF systems. Therefore, Hu et al.'s modeling is unsuitable for TADF systems, which has motivated us to introduce the new approach described in this study.

To validate the reliability of our strategy for other TADF molecular systems, we performed an additional experiment using this method for a well-known TADF molecule, 4CzIPN, whose fluorescence quantum yield (Φ_F) was reported to be

93.8%.[4] The transient fluorescence kinetics of 4CzIPN is shown in Figure 4, and Table 5 summarizes the dynamic decay parameters and ΔE_{S-T} in deoxygenated toluene at room temperature.
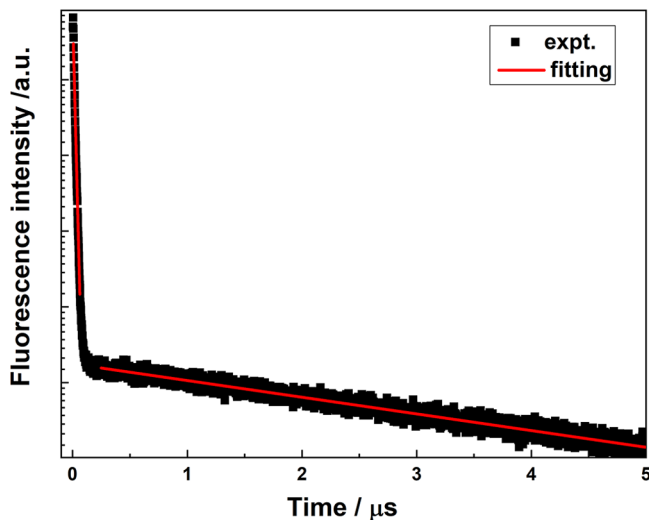
Figure 4. Fluorescence emission kinetics of 4CzIPN (1×10^{-5} M) in deoxygenated toluene, at room temperature and $\lambda_{ex} = 380$ nm, and with the emission detected at 507 nm.

The two components of prompt and delayed fluorescence emissions were observed clearly in Figure 4. From the biexponential fitting, τ_{PF} and τ_{DF} were determined to be 13.4 and 2688 ns, respectively. Using the I_{PF}/I_{DF} proportion and our modeling, we finally obtained the corresponding rates and energy gap for 4CzIPN, $k_{ISC} = 5.42 \times 10^7$ s^{-1}, $k_{RISC} = 1.09 \times 10^6$ s^{-1}, and $\Delta E_{S-T} = 72$ meV. This energy gap is slightly lower than the previous result (83 meV in CBP films).[4] However, the previously reported value actually was the activation energy from the T_1 to S_1 state,[4] which deservedly was slightly higher than the real energy gap.

Additionally, in contrast to another widely used approach to calculate ΔE_{S-T} using temperature-dependent photoluminescence measurements,[24−27] no stringent condition of $k_{ISC} \gg k_F$ is demanded in our method, and a more modest assumption of $(k_S - k_T)^2 \gg 4k_{ISC}\cdot k_{RISC}$ is requested. Thus, our strategy can be suitable for the systems in which k_{ISC} is comparable with the fluorescence emission rate (k_F). Moreover, since in our method the k_S, k_T, and $k_{ISC}\cdot k_{RISC}$ values are determined by fitting transient fluorescence kinetics with a biexponential function, it will be invalidated if the prompt fluorescence is entirely quenched. Therefore, our approach and the temperature-dependent photoluminescence lifetime measurements are complementary to each other.

In summary, we introduce a new, facile yet robust approach to precisely determine energy gap (i.e., ΔE_{S-T}) in TADF systems using a recently reported DMACPDO molecule as a representative. Explicit modeling has been conducted to meaningfully physically describe this singlet−triplet coupling

system in which the decay of singlet-excited DMACPDO is expected to occur biexponentially. Based on fitting the kinetics of transient fluorescence emission together with a thermal-equilibrium approximation of S_1 and T_1 populations, the elusive ISC and RISC rates can be extracted and the ΔE_{S-T} value is then determined. Moreover, our modeling and corresponding results perfectly explain the unusual experimental results of DMACPDO fluorescence: an opposite trend was observed in its fluorescence intensity with solvent polarity under air-saturated and deoxygenated conditions. Our approach can be readily extended to other similar TADF systems like 4CzIPN to precisely determine the crucial parameter of ΔE_{S-T}. Therefore, a deeper understanding of the energy-loss mechanisms involved in the related photo-conversion process can be achieved.

■ EXPERIMENTAL AND COMPUTATIONAL METHODS

Steady-state UV−vis absorption spectra were recorded with a spectrophotometer (UV-3600; Shimadzu) at room temperature (298 K). Photoluminescence spectra were measured at room temperature with a fluorescence spectrophotometer (F-4600; Hitachi). Time-dependent fluorescence emission dynamics were obtained by a spectrometer (FluoTime 300; PicoQuant, GmbH) with a picosecond pulsed laser (LAS-TER480; PicoQuant) as the photoexcitation source. Using perylene as a standard, steady-state absorbance spectra of the sample and a standard in diluted solutions were recorded using a fluorescence spectrometer, where their absorbance at the excitation wavelength was no more than 0.05. By integrating the band area in the emission spectra of the sample or standard, the quantum yield of the sample could be determined. In the current experiments, the fluorescence quantum yield, Φ_F, was calculated using eq 8 and taking into account $\Phi_{std} = 71.0\%$ in toluene[61]

$$\Phi_F = \Phi_{std}\left(\frac{A_{std}}{I_{std}}\right)\left(\frac{I_{sam}}{A_{sam}}\right)\left(\frac{\eta_{sam}}{\eta_{std}}\right)^2 \tag{8}$$

where A, I, and η are the absorbance intensities, integrated luminescence intensities, and refractive indices of the solvents used for the standard and samples, respectively. All quantum chemical calculations were performed with the Gaussian 16 program suite.[62] For all of the DFT calculations, def2-tzvp basis sets[63] were used for geometry optimization and excitation energy computations. The harmonic vibrational frequencies were calculated at the same levels of theory to verify optimized structures and calculate zero-point energies.

■ ASSOCIATED CONTENT

Ⓢⓘ Supporting Information

The Supporting Information is available free of charge at https://pubs.acs.org/doi/10.1021/acs.jpclett.2c00428.

Optimized geometrical parameters and excitation energies of DMACPDO in the S_0, S_1, and T_1 states; details of modeling formulation; fitting the kinetics of

Table 5. Dynamic Decay Parameters of 4CzIPN (S_1) in Deoxygenated Toluene at Room Temperature

	I_{PF}/I_{DF}	k_F ($\times 10^7$ s^{-1})	k_{ISC} ($\times 10^7$ s^{-1})	k_{RISC} ($\times 10^6$ s^{-1})	ΔE_{S-T} (meV)
4C$_Z$IPN	0.29/0.71	2.03 ± 0.04^a	$5.42 \pm 0.04,^a$ 4.00^b	$1.09 \pm 0.01,^a$ 1.29^b	$72 \pm 1,^a$ 83^b

^{a}The present results. ^{b}From ref 4, in CBP films.

transient fluorescence intensity; thermal equilibrium analysis; and Cartesian coordinates of optimized geometries of DMACPDO in the S_0, S_1, and T_1 states at the BMK/def2-tzvp level (PDF)

◼ AUTHOR INFORMATION

Corresponding Authors

Xiaoguo Zhou − *Hefei National Laboratory for Physical Sciences at the Microscale, Department of Chemical Physics, University of Science and Technology of China, Hefei, Anhui 230026, China;* ⓞ orcid.org/0000-0002-0264-0146; Email: xzhou@ustc.edu.cn

Lin Chen − *School of Physics and Materials Engineering, Hefei Normal University, Hefei, Anhui 230601, China;* Email: chenlin@hfnu.edu.cn

Authors

Min Zheng − *Hefei National Laboratory for Physical Sciences at the Microscale, Department of Chemical Physics, University of Science and Technology of China, Hefei, Anhui 230026, China*

Yuanming Li − *Hefei National Laboratory for Physical Sciences at the Microscale, Department of Chemical Physics, University of Science and Technology of China, Hefei, Anhui 230026, China*

Yaxiong Wei − *School of Physics and Electronic Information, Anhui Normal University, Wuhu, Anhui 241000, China*

Shilin Liu − *Hefei National Laboratory for Physical Sciences at the Microscale, Department of Chemical Physics, University of Science and Technology of China, Hefei, Anhui 230026, China*

Complete contact information is available at:
https://pubs.acs.org/10.1021/acs.jpclett.2c00428

Author Contributions

‖M.Z. and Y.L. contributed equally to this work.

Notes

The authors declare no competing financial interest.

◼ REFERENCES

(1) Tao, Y.; Yuan, K.; Chen, T.; Xu, P.; Li, H.; Chen, R.; Zheng, C.; Zhang, L.; Huang, W. Thermally Activated Delayed Fluorescence Materials Towards the Breakthrough of Organoelectronics. *Adv. Mater.* **2014**, *26*, 7931−7958.

(2) Berberan-Santos, M. N.; Garcia, J. M. M. Unusually Strong Delayed Fluorescence of C70. *J. Am. Chem. Soc.* **1996**, *118*, 9391−9394.

(3) Endo, A.; Ogasawara, M.; Takahashi, A.; Yokoyama, D.; Kato, Y.; Adachi, C. Thermally Activated Delayed Fluorescence from Sn^{4+}−Porphyrin Complexes and Their Application to Organic Light Emitting Diodes — A Novel Mechanism for Electroluminescence. *Adv. Mater.* **2009**, *21*, 4802−4806.

(4) Uoyama, H.; Goushi, K.; Shizu, K.; Nomura, H.; Adachi, C. Highly efficient organic light-emitting diodes from delayed fluorescence. *Nature* **2012**, *492*, 234−238.

(5) Yang, Z.; Mao, Z.; Xie, Z.; Zhang, Y.; Liu, S.; Zhao, J.; Xu, J.; Chi, Z.; Aldred, M. P. Recent advances in organic thermally activated delayed fluorescence materials. *Chem. Soc. Rev.* **2017**, *46*, 915−1016.

(6) Yang, Z.; Mao, Z.; Xu, C.; Chen, X.; Zhao, J.; Yang, Z.; Zhang, Y.; Wu, W.; Jiao, S.; Liu, Y.; Aldred, M. P.; Chi, Z. A sterically hindered asymmetric D−A−D′ thermally activated delayed fluorescence emitter for highly efficient non-doped organic light-emitting diodes. *Chem. Sci.* **2019**, *10*, 8129−8134.

(7) Wu, Y.; Zhao, Y.; Zhou, P.; Zheng, D.; Wang, H.; Tang, S.; Tian, J.; Yang, S.; Deng, W.; Han, K.; Song, F. Enhancing Intersystem Crossing to Achieve Thermally Activated Delayed Fluorescence in a Water-Soluble Fluorescein Derivative with a Flexible Propenyl Group. *J. Phys. Chem. Lett.* **2020**, *11*, 5692−5698.

(8) Liu, S.; Yang, B.; Chen, J.; Wei, D.; Zheng, D.; Kong, Q.; Deng, W.; Han, K. Efficient Thermally Activated Delayed Fluorescence from All-Inorganic Cesium Zirconium Halide Perovskite Nanocrystals. *Angew. Chem., Int. Ed.* **2020**, *59*, 21925−21929.

(9) Endo, A.; Sato, K.; Yoshimura, K.; Kai, T.; Kawada, A.; Miyazaki, H.; Adachi, C. Efficient up-conversion of triplet excitons into a singlet state and its application for organic light emitting diodes. *Appl. Phys. Lett.* **2011**, *98*, 083302.

(10) Goushi, K.; Yoshida, K.; Sato, K.; Adachi, C. Organic light-emitting diodes employing efficient reverse intersystem crossing for triplet-to-singlet state conversion. *Nat. Photonics* **2012**, *6*, 253−258.

(11) Sato, K.; Shizu, K.; Yoshimura, K.; Kawada, A.; Miyazaki, H.; Adachi, C. Organic Luminescent Molecule with Energetically Equivalent Singlet and Triplet Excited States for Organic Light-Emitting Diodes. *Phys. Rev. Lett.* **2013**, *110*, 247401.

(12) Dias, F. B.; Bourdakos, K. N.; Jankus, V.; Moss, K. C.; Kamtekar, K. T.; Bhalla, V.; Santos, J.; Bryce, M. R.; Monkman, A. P. Triplet Harvesting with 100% Efficiency by Way of Thermally Activated Delayed Fluorescence in Charge Transfer OLED Emitters. *Adv. Mater.* **2013**, *25*, 3707−3714.

(13) An, J.; Wu, Y.; Lu, M.; Han, K.; Song, F.; Peng, X. Long-wavelength chromophores with thermally activated delayed fluorescence based on fluorescein derivatives. *Journal of Photonics for Energy* **2018**, *8*, 032103.

(14) Liu, Y.; Li, C.; Ren, Z.; Yan, S.; Bryce, M. R. All-organic thermally activated delayed fluorescence materials for organic light-emitting diodes. *Nature Reviews Materials* **2018**, *3*, 18020.

(15) Li, C.; Nobuyasu, R. S.; Wang, Y.; Dias, F. B.; Ren, Z.; Bryce, M. R.; Yan, S. Solution-Processable Thermally Activated Delayed Fluorescence White OLEDs Based on Dual-Emission Polymers with Tunable Emission Colors and Aggregation-Enhanced Emission Properties. *Advanced Optical Materials* **2017**, *5*, 1700435.

(16) Wu, K.; Zhang, T.; Wang, Z.; Wang, L.; Zhan, L.; Gong, S.; Zhong, C.; Lu, Z.-H.; Zhang, S.; Yang, C. De Novo Design of Excited-State Intramolecular Proton Transfer Emitters via a Thermally Activated Delayed Fluorescence Channel. *J. Am. Chem. Soc.* **2018**, *140*, 8877−8886.

(17) Chen, J.-X.; Xiao, Y.-F.; Wang, K.; Sun, D.; Fan, X.-C.; Zhang, X.; Zhang, M.; Shi, Y.-Z.; Yu, J.; Geng, F.-X.; Lee, C.-S.; Zhang, X.-H. Managing Locally Excited and Charge-Transfer Triplet States to Facilitate Up-Conversion in Red TADF Emitters That Are Available for Both Vacuum- and Solution-Processes. *Angew. Chem., Int. Ed.* **2021**, *60*, 2478−2484.

(18) Xie, F.-M.; Zeng, X.-Y.; Zhou, J.-X.; An, Z.-D.; Wang, W.; Li, Y.-Q.; Zhang, X.-H.; Tang, J.-X. Intramolecular H-bond design for efficient orange−red thermally activated delayed fluorescence based on a rigid dibenzo[f,h]pyrido[2,3-b]quinoxaline acceptor. *Journal of Materials Chemistry C* **2020**, *8*, 15728−15734.

(19) Berenis, D.; Kreiza, G.; Juršėnas, S.; Kamarauskas, E.; Ruibys, V.; Bobrovas, O.; Adomėnas, P.; Kazlauskas, K. Different RISC rates in benzoylpyridine-based TADF compounds and their implications for solution-processed OLEDs. *Dyes Pigm.* **2020**, *182*, 108579.

(20) Ma, F.; Zhao, X.; Ji, H.; Zhang, D.; Hasrat, K.; Qi, Z. Molecular engineering of dendritic luminogens with thermally activated delayed fluorescence and aggregation-induced emission characteristics for efficient solution-processed non-doped OLEDs. *Journal of Materials Chemistry C* **2020**, *8*, 12272−12283.

(21) Wang, P.; Yu, J.; Chen, S.; Yu, H.; Yan, X.; Guan, Y.; Chen, J.; Li, L. 3-Benzoyl-4H-chromen-4-one: A novel twisted acceptor for highly efficient thermally activated delayed fluorescence emitters. *Dyes Pigm.* **2020**, *183*, 108744.

(22) Hatakeyama, T.; Shiren, K.; Nakajima, K.; Nomura, S.; Nakatsuka, S.; Kinoshita, K.; Ni, J.; Ono, Y.; Ikuta, T. Ultrapure Blue Thermally Activated Delayed Fluorescence Molecules: Efficient HOMO−LUMO Separation by the Multiple Resonance Effect. *Adv. Mater.* **2016**, *28*, 2777−2781.

(23) Vandewal, K.; Benduhn, J.; Nikolis, V. C. How to determine optical gaps and voltage losses in organic photovoltaic materials. *Sustainable Energy Fuels* **2018**, *2*, 538−544.

(24) Parker, C. A.; Hatchard, C. G. Triplet-singlet emission in fluid solutions. Phosphorescence of eosin. *Trans. Faraday Soc.* **1961**, *57*, 1894−1904.

(25) Kirchhoff, J. R.; Gamache, R. E.; Blaskie, M. W.; Del Paggio, A. A.; Lengel, R. K.; McMillin, D. R. Temperature dependence of luminescence from Cu(NN)2+ systems in fluid solution. Evidence for the participation of two excited states. *Inorg. Chem.* **1983**, *22*, 2380−2384.

(26) Hofbeck, T.; Monkowius, U.; Yersin, H. Highly Efficient Luminescence of Cu(I) Compounds: Thermally Activated Delayed Fluorescence Combined with Short-Lived Phosphorescence. *J. Am. Chem. Soc.* **2015**, *137*, 399−404.

(27) Liu, S.; Yang, B.; Chen, J.; Wei, D.; Zheng, D.; Kong, Q.; Deng, W.; Han, K. Efficient Thermally Activated Delayed Fluorescence from All-Inorganic Cesium Zirconium Halide Perovskite Nanocrystals. *Angew. Chem., Int. Ed.* **2020**, *59*, 21925−21929.

(28) Lv, X.; Wang, Y.; Li, N.; Cao, X.; Xie, G.; Huang, H.; Zhong, C.; Wang, L.; Yang, C. Regulating the photophysical properties of highly twisted TADF emitters by concurrent through-space/-bond charge transfer. *Chem. Eng. J.* **2020**, *402*, 126173.

(29) Narsaria, A. K.; Rauch, F.; Krebs, J.; Endres, P.; Friedrich, A.; Krummenacher, I.; Braunschweig, H.; Finze, M.; Nitsch, J.; Bickelhaupt, F. M.; Marder, T. B. Computationally Guided Molecular Design to Minimize the LE/CT Gap in D-π-A Fluorinated Triarylboranes for Efficient TADF via D and π-Bridge Tuning. *Adv. Funct. Mater.* **2020**, *30*, 2002064.

(30) Xu, S.; Yang, Q.; Wan, Y.; Chen, R.; Wang, S.; Si, Y.; Yang, B.; Liu, D.; Zheng, C.; Huang, W. Predicting intersystem crossing efficiencies of organic molecules for efficient thermally activated delayed fluorescence. *Journal of Materials Chemistry C* **2019**, *7*, 9523−9530.

(31) Al-Saadon, R.; Sutton, C.; Yang, W. Accurate Treatment of Charge-Transfer Excitations and Thermally Activated Delayed Fluorescence Using the Particle−Particle Random Phase Approximation. *J. Chem. Theory Comput.* **2018**, *14*, 3196−3204.

(32) Dhara, A. K.; Ghosh, S. K. Density-functional theory for time-dependent systems. *Phys. Rev. A Gen Phys.* **1987**, *35*, 442−444.

(33) Marques, M. A. L.; Gross, E. K. U. TIME-DEPENDENT DENSITY FUNCTIONAL THEORY. *Annu. Rev. Phys. Chem.* **2004**, *55*, 427−455.

(34) Wang, Y.; Zhao, H.; Yang, C.; Jie, J.; Dai, X.; Zhou, Q.; Liu, K.; Song, D.; Su, H. Degradation of Cytosine Radical Cations in 2′-Deoxycytidine and in i-Motif DNA: Hydrogen-Bonding Guided Pathways. *J. Am. Chem. Soc.* **2019**, *141*, 1970−1979.

(35) Im, Y.; Kim, M.; Cho, Y. J.; Seo, J.-A.; Yook, K. S.; Lee, J. Y. Molecular Design Strategy of Organic Thermally Activated Delayed Fluorescence Emitters. *Chem. Mater.* **2017**, *29*, 1946−1963.

(36) Xue, Y.; Dou, Y.; An, L.; Zheng, Y.; Zhang, L.; Liu, Y. Electronic structure and spectral properties of aurones as visible range fluorescent probes: a DFT/TDDFT study. *RSC Adv.* **2016**, *6*, 7002−7010.

(37) Goerigk, L.; Grimme, S. Assessment of TD-DFT methods and of various spin scaled CIS(D) and CC2 versions for the treatment of low-lying valence excitations of large organic dyes. *J. Chem. Phys.* **2010**, *132*, 184103.

(38) Silva-Junior, M. R.; Schreiber, M.; Sauer, S. P. A.; Thiel, W. Benchmarks for electronically excited states: Time-dependent density functional theory and density functional theory based multireference configuration interaction. *J. Chem. Phys.* **2008**, *129*, 104103.

(39) Dwyer, A. D.; Tozer, D. J. Effect of chemical change on TDDFT accuracy: orbital overlap perspective of the hydrogenation of retinal. *Phys. Chem. Chem. Phys.* **2010**, *12*, 2816−2818.

(40) Jacquemin, D.; Wathelet, V.; Perpète, E. A.; Adamo, C. Extensive TD-DFT Benchmark: Singlet-Excited States of Organic Molecules. *J. Chem. Theory Comput.* **2009**, *5*, 2420−2435.

(41) Sun, H.; Zhong, C.; Brédas, J.-L. Reliable Prediction with Tuned Range-Separated Functionals of the Singlet−Triplet Gap in Organic Emitters for Thermally Activated Delayed Fluorescence. *J. Chem. Theory Comput.* **2015**, *11*, 3851−3858.

(42) Penfold, T. J. On Predicting the Excited-State Properties of Thermally Activated Delayed Fluorescence Emitters. *J. Phys. Chem. C* **2015**, *119*, 13535−13544.

(43) Wong, M. Y.; Zysman-Colman, E. Purely Organic Thermally Activated Delayed Fluorescence Materials for Organic Light-Emitting Diodes. *Adv. Mater.* **2017**, *29*, 1605444.

(44) Zhang, Q.; Kuwabara, H.; Potscavage, W. J.; Huang, S.; Hatae, Y.; Shibata, T.; Adachi, C. Anthraquinone-Based Intramolecular Charge-Transfer Compounds: Computational Molecular Design, Thermally Activated Delayed Fluorescence, and Highly Efficient Red Electroluminescence. *J. Am. Chem. Soc.* **2014**, *136*, 18070−18081.

(45) Christian, R.; Thomas, W. Solvent Effects on the Absorption Spectra of Organic Compounds. *Solvents and Solvent Effects in Organic Chemistry*; Wiley-VCH Verlag GmbH & Co. KGaA: 2010; pp 359−424..

(46) Becke, A. D. Density-functional thermochemistry. III. The role of exact exchange. *J. Chem. Phys.* **1993**, *98*, 5648−5652.

(47) Stephens, P. J.; Devlin, F. J.; Chabalowski, C. F.; Frisch, M. J. Ab Initio Calculation of Vibrational Absorption and Circular Dichroism Spectra Using Density Functional Force Fields. *J. Phys. Chem.* **1994**, *98*, 11623−11627.

(48) Adamo, C.; Scuseria, G. E.; Barone, V. Accurate excitation energies from time-dependent density functional theory: Assessing the PBE0 model. *J. Chem. Phys.* **1999**, *111*, 2889−2899.

(49) Perdew, J. P.; Burke, K.; Ernzerhof, M. Generalized Gradient Approximation Made Simple. *Phys. Rev. Lett.* **1996**, *77*, 3865−3868.

(50) Boese, A. D.; Martin, J. M. L. Development of density functionals for thermochemical kinetics. *J. Chem. Phys.* **2004**, *121*, 3405−3416.

(51) Zhao, Y.; Truhlar, D. G. The M06 suite of density functionals for main group thermochemistry, thermochemical kinetics, non-covalent interactions, excited states, and transition elements: two new functionals and systematic testing of four M06-class functionals and 12 other functionals. *Theor. Chem. Acc.* **2008**, *120*, 215−241.

(52) Zhang, X.; Jie, J.; Song, D.; Su, H. Deprotonation of Guanine Radical Cation G•+ Mediated by the Protonated Water Cluster. *J. Phys. Chem. A* **2020**, *124*, 6076−6083.

(53) Yanai, T.; Tew, D. P.; Handy, N. C. A new hybrid exchange−correlation functional using the Coulomb-attenuating method (CAM-B3LYP). *Chem. Phys. Lett.* **2004**, *393*, 51−57.

(54) Iikura, H.; Tsuneda, T.; Yanai, T.; Hirao, K. A long-range correction scheme for generalized-gradient-approximation exchange functionals. *J. Chem. Phys.* **2001**, *115*, 3540−3544.

(55) Yang, C.; Su, H.; Sun, X.; George, M. W. Ultrafast formation of the benzoic acid triplet upon ultraviolet photolysis and its sequential photodissociation in solution. *J. Chem. Phys.* **2012**, *136*, 204507.

(56) Turro, J. N. *Modern Molecular Photochemistry*; University Science Books: Sausalito, CA, 1991.

(57) Ishimatsu, R.; Matsunami, S.; Shizu, K.; Adachi, C.; Nakano, K.; Imato, T. Solvent Effect on Thermally Activated Delayed

Fluorescence by 1,2,3,5-Tetrakis(carbazol-9-yl)-4,6-dicyanobenzene. *J. Phys. Chem. A* **2013**, *117*, 5607−5612.

(58) Masui, K.; Nakanotani, H.; Adachi, C. Analysis of exciton annihilation in high-efficiency sky-blue organic light-emitting diodes with thermally activated delayed fluorescence. *Org. Electron.* **2013**, *14*, 2721−2726.
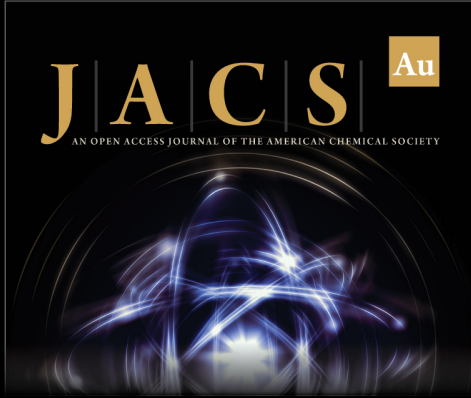
(59) Zhang, Q.; Li, B.; Huang, S.; Nomura, H.; Tanaka, H.; Adachi, C. Efficient blue organic light-emitting diodes employing thermally activated delayed fluorescence. *Nat. Photonics* **2014**, *8*, 326−332.

(60) Hu, J.; Zhang, Q.; Luo, Y. Retrieving the Rate of Reverse Intersystem Crossing from Ultrafast Spectroscopy. *J. Phys. Chem. Lett.* **2016**, *7*, 3908−3912.

(61) Olmsted, J. Calorimetric determinations of absolute fluorescence quantum yields. *J. Phys. Chem.* **1979**, *83*, 2581−2584.

(62) Frisch, M. J.; Trucks, G. W.; Schlegel, H. B.; Scuseria, G. E.; Robb, M. A.; Cheeseman, J. R.; Scalmani, G.; Barone, V.; Petersson, G. A.; Nakatsuji, H.; Li, X.; Caricato, M.; Marenich, A. V.; Bloino, J.; Janesko, B. G.; Gomperts, R.; Mennucci, B.; Hratchian, H. P.; Ortiz, J. V.; Izmaylov, A. F.; Sonnenberg, J. L.; Williams-Young, D.; Ding, F.; Lipparini, F.; Egidi, F.; Goings, J.; Peng, B.; Petrone, A.; Henderson, T.; Ranasinghe, D.; Zakrzewski, V. G.; Gao, J.; Rega, N.; Zheng, G.; Liang, W.; Hada, M.; Ehara, M.; Toyota, K.; Fukuda, R.; Hasegawa, J.; Ishida, M.; Nakajima, T.; Honda, Y.; Kitao, O.; Nakai, H.; Vreven, T.; Throssell, K.; Montgomery, J. A., Jr.; Peralta, J. E.; Ogliaro, F.; Bearpark, M. J.; Heyd, J. J.; Brothers, E. N.; Kudin, K. N.; Staroverov, V. N.; Keith, T. A.; Kobayashi, R.; Normand, J.; Raghavachari, K.; Rendell, A. P.; Burant, J. C.; Iyengar, S. S.; Tomasi, J.; Cossi, M.; Millam, J. M.; Klene, M.; Adamo, C.; Cammi, R.; Ochterski, J. W.; Martin, R. L.; Morokuma, K.; Farkas, O.; Foresman, J. B.; Fox, D. J. *Gaussian 16*, revision C.01; Gaussian, Inc.: Wallingford, CT, 2016.

(63) Weigend, F.; Ahlrichs, R. Balanced basis sets of split valence, triple zeta valence and quadruple zeta valence quality for H to Rn: Design and assessment of accuracy. *Phys. Chem. Chem. Phys.* **2005**, *7*, 3297−3305.